Engineered Science
DOI: https://dx.doi.org/10.30919/es1869

Magnet-Free Optical Tesla Valve in Photonic Crystal Cavity-Waveguides and Experimental Demonstration

Asrafali Barkathulla,[1,3] Fahim Khan,[1,3] Deepika Tyagi,[1,3] Mi Lin,[1] Qiong Wang,[1] Keyu Tao,[1] Yogesh Natesan,[2] Suling Shen,[4,5] Qiang Liu[6,*] and Zhengbiao Ouyang[1,3,*]

Abstract

The unidirectional transmission of electromagnetic (EM) waves based on Faraday rotation typically involves magnetic materials, which limits the integration of such devices at the chip level. Sparked by the wave-particle duality of electromagnetic waves in quantum theory and by the unidirectional transportation property of conventional fluidic Tesla valve (FTV), we proposed and demonstrated numerically and experimentally an optical Tesla valve (OTV) comprising photonic crystal cavity-waveguides entirely using magnet-free dielectrics. Spatial-reversal symmetry is broken, which, for a photon stream, is equivalent to apparent time-reversal symmetry breaking that is responsible for the unidirectional transmission property of the proposed OTV. The realized OTV exhibits a unidirectional transmission with a stopping factor of more than 40 dB at the microwave frequency. The proposed cavity-waveguide system is made of a single photonic crystal rather than multiple periodic structures. The experimentally demonstrated OTV has potential applications in optical, photonic, and quantum optics technologies, opening up a new way to control electromagnetic waves and other waves, such as acoustic waves, pressure waves, and soliton waves.

Keywords: Unidirectional wave transport; Optical tesla valve; Optical photonic crystals; Optical diode.
Received: 12 September 2025; Revised: 29 October 2025; Accepted: 12 November 2025
Article type: Research article.

1. Introduction

Unidirectional energy/field/signal transport gains primary interest in the fields of quantum computing,[1] signal processing,[2] medical imaging,[3] and satellite and aerospace applications.[4] Metamaterials (MTM) and photonic crystals (PhCs) are readily available candidates for designing and demonstrating electromagnetic (EM) wave transmission due to their intriguing EM properties. The first PhC one-way waveguide was realized and demonstrated in the early 21st century by Haldane et.al.[5] However, all these devices were demonstrated using non-linear, magnetic materials[6–14] in which the Lorentz reciprocity theorem no longer holds, and also time-reversal symmetry is broken.

Recently, researchers have demonstrated the possibility of unidirectional transmission using purely passive, linear, and non-magnetic materials without violating the Lorentz reciprocity theorem or breaking time-reversal symmetry. It is worth mentioning that the unidirectional and nonreciprocal transmission phenomena need not be the same (a plethora of debate is found in literature[15–19]), where the latter inhibits the unidirectional transmission in linear and passive materials due to the symmetric zero half-diagonal element present in the constituent parameters of the linear and time-independent materials. But using PhC band-matching techniques[20,21] and a machine learning algorithm,[22] unidirectional transmission has been reported using only linear and passive media.

The main principle of unidirectional transmission in PhCs with linear and passive materials involves mode scattering, as well as the quantum perspective of wave-particle duality, which renders the photon (particle-like) nature for the incident EM waves inside the PhC system, where the spatial inversion symmetry is broken, which is indeed apparently equivalent to breaking the time reversal symmetry in the magnetic

[1]*Key Laboratory of Optoelectronic Devices and Systems of Ministry of Education and Guangdong Province, College of Physics and Optoelectronic Engineering, Shenzhen University, Shenzhen, 518060, China*
[2]*Metamaterials and Photonic Structures Laboratory, Department of Physics, National Institute of Technology Calicut, Kozhikode, 673601, India*

anisotropic media. While considering the mode scattering in which forward/backward wave propagations involve different coupling of scattered electromagnetic waves in a system made of two different periodic structures, the system as a whole is overall reciprocal, linear, and passive.

Rather than combining two different periodic systems with band matching, we explore the problem of unidirectional transmission from the Tesla valve concept.

Tesla proposed an influential unidirectional fluid device known as a vascular conduct or a fluidic Tesla valve (FTV).[23] Some of the outcomes of the FTV in the various domains include thermal management, regulation using the capillary structure, and an activated FTV,[24] improving the pressure suppression feedback and backflow combustion product,[25] microfluidic diodes for turbulence and pulsatile flow enhancement,[26,27] micromixer performance enhancement,[28,29] proton exchange membrane fuel cell flow field studies,[30] dual-mode and dual-target biosensor regulation,[31] liquid multistage FTV,[32] Tesla valve (TV) capillary heat dissipation channel, and reverse TV channel aimed at mitigating the eddy current issue at bends inside the capillary bionic flow channel,[33] and improving the efficiency of the heat transfer with the TV through multilayer perception models.[34] Notably, the valve design involved no moving machinery. However, the design of FTVs lacks practical significance due to their relatively poor fluid-blocking effect in the reverse direction in fluid dynamics.[35] The equivalence between fluid flow and EM wave transport can be well understood by the equivalence between Maxwell's wave equation and the solution to the Navier-Stokes equations.[36] In magnetohydrodynamics, the EM fields are modelled as fluids; therefore, a dynamical analytical model for the optical Tesla valve (OTV) can be implemented for EM wave flow.[37] In this work, we demonstrate the OTV for the EM waves. The analytical formalism for the EM fluid model was used to explain the unidirectional transport of EM waves in the modelled OTV. In parallel, extensive studies on electromagnetic interference (EMI) shielding[38,39] have focused on broadband suppression of unwanted signals, but unlike such isotropic attenuation strategies, our OTV design achieves selective, high-contrast one-way transmission. The finite element-based numerical simulations were carried out to realize the proposed design. An experimental analysis was conducted to validate the numerical studies at the microwave band. It is worth mentioning that unidirectional (asymmetric) transmission can be applied for optical isolation; however, they operate through different mechanisms. Besides the application for unidirectional transmission as isolators, it can also find applications in polarization control, directional filtering or spatial filtering, and asymmetric light routing.

2. Materials and methods

2.1 Design and simulation of the PhC based OTV

The unit-cell of the square-lattice photonic crystal (PhC) was designed as shown in Fig. 1(a) with a rod radius 'r' of 0.2223a, the lattice constant 'a' is 1.8 cm. It is evident from the band diagram shown in Fig. 1(b) that the band gap spans about ~ 3 GHz, for the transverse electric (TE) polarization. Utilizing the plane-wave expansion method,[40] the band calculations were carried out along the irreducible Brillouin zone as shown in Fig. 1(a), which is the shaded triangular region that spans the line trace along the highest symmetry points Γ-M-K-Γ. These highest symmetry points were chosen due to the geometrical isotropy presented in the unit cell of the designed PhC. The rod is assigned with alumina (Al_2O_3) (ε_r = 9.39, μ_r = 1) for numerical calculations. It is well known that the bandgap can be scaled to the desired frequency range according to the required applications by varying the PhC rod's radius, lattice parameter, and refractive index.[41]

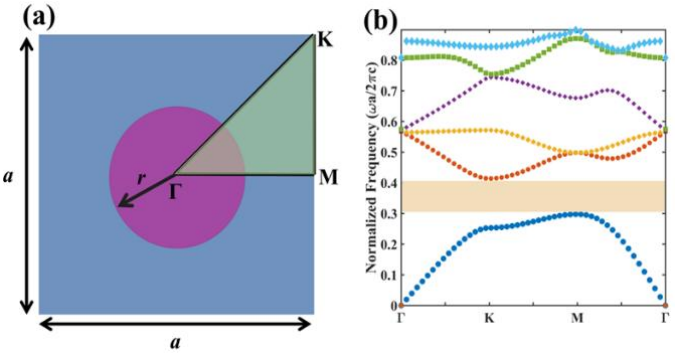

Fig. 1: Unit-cell and band map. (a) The designed PhC unit-cell with radius (r) = 3.8 mm. (b) Band diagram of the designed PhC array.

The line defect was created to demonstrate the perfect reciprocal effect in the linear waveguide design in the bandgap region, as shown in Fig. 2. As expected, the linear PhC waveguide has no interference effect to stop the reverse transmission. In contrast, the designed OTV in Fig. 3 has a stopping impact due to its geometrical design, and the underpinned principles were further discussed.

[3]*THz Technology Laboratory, Shenzhen Key Laboratory of Micro-nano Photonic Information Technology, Shenzhen University, Shenzhen, 518060, China*

[4]*State Key Laboratory of Intelligent Construction and Healthy Operation and Maintenance of Deep Underground Engineering, College of Civil and Transportation Engineering, Shenzhen University, Shenzhen, 518060, China*

[5]*DGUT-CNAM Institute, Dongguan University of Technology, Dongguan, 523808, China*

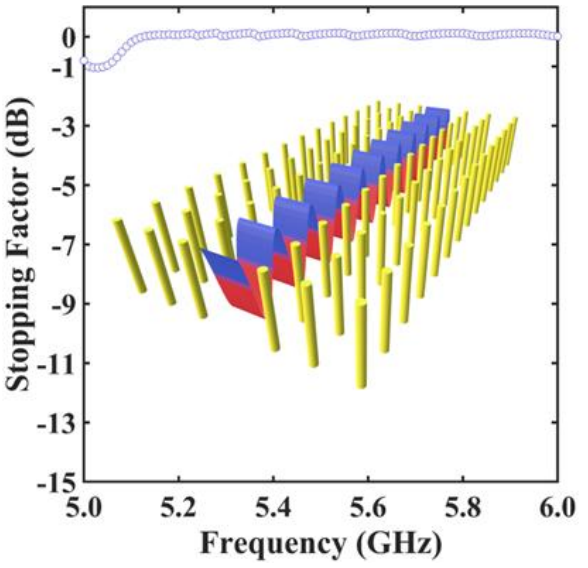

Fig. 2: Illustration of the linear PhC waveguide stopping factor (SF), the insert shows the E_z component of the incident electric field. The definition of SF is given in Eq. (1) in the following.

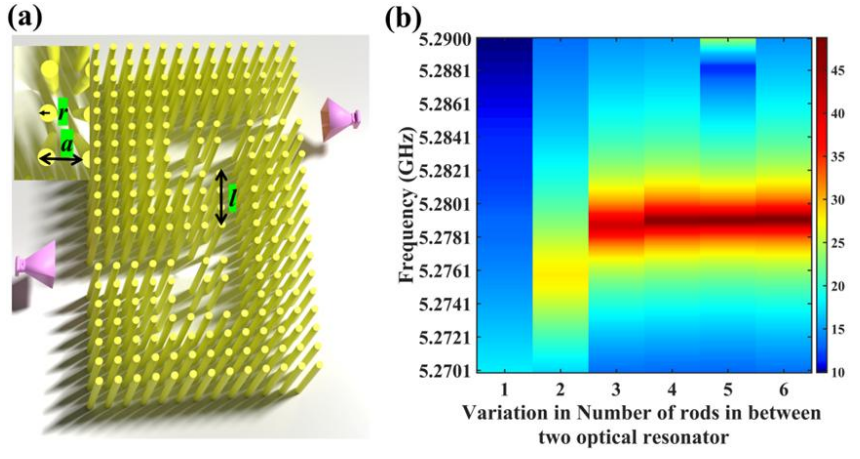

Fig. 3: OTV design and optimization. (a) OTV with two optical resonators and a linear PhC waveguide with waveguide length '*l*', radius of the rod '*r*' of 3.8 mm, and lattice constant '*a*' of 1.8 cm. (b) The color map shows the variation of the SF with the varying '*l*'. (Colorbar shows the electric field -z component E_z).

As mentioned, the designed OTV is an inspiration from the conventional FTV, where the fluid flow is stopped in the reverse direction without any physically moving mechanical parts, and only allows the forward flow. This inspiration is intuitively matched with the optical wave control and gives rise to a novel OTV. The design for the FTV is not limited to the proposed design of OTVs; it could open up a new mechanism in the domain of unidirectional transport of EM waves, acoustic waves, pressure waves, soliton waves, and so on.

The OTV using a square-lattice PhC was designed by removing some rods in a PhC, as shown in Fig. 3, solely inspired by the design requirements of the FTV.[23] The modelled OTV has three major segments, as shown in Fig. 3(a), including two optical circular waveguide cavities interconnected with a linear PhC waveguide. The core idea of the inclusion of the optical circular waveguide cavity in the design is to establish the interference effect, which supports the forward flow and blocks the reverse flow. The added linear PhC waveguide connecting two optical circular waveguide cavities is to feed the constructively interfered wave into the second optical circular waveguide cavity to establish another round of optical interference. The same criterion is applicable for the reverse flow, except that destructive interference exists rather than constructive interference to prohibit the reverse flow. The length of the linear waveguide was optimized to achieve the required blocking effect, as shown in Fig. 3(b). Furthermore, to establish this blocking effect, the forward propagation and the reverse blocking are shown in Fig. 4. It is

[6]*School of Life and Health Technology, Dongguan University of Technology, Dongguan, Guangdong, 523808, China*
[*]*Email:* 2025033@dgut.edu.cn (Qiang Liu),
zbouyang@szu.edu.cn (Zhengbiao Ouyang)

evident from Fig. 4 that the normalized value at 5.279 GHz shows maximum field intensity ($|E|^2$ $(V/m)^2$) for forward operation and nearly zero for reverse blocking.

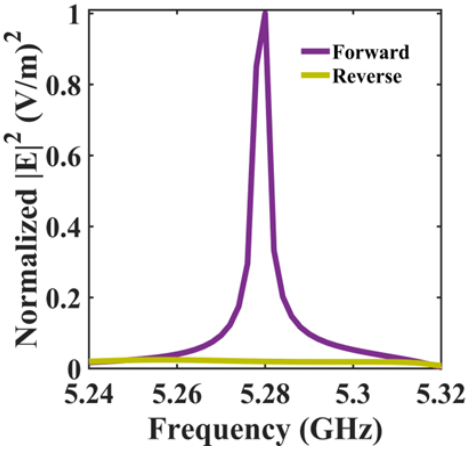

Fig. 4: Illustration of the normalized $|E|^2$ for forward flow and reverse blocking effect arising from the designed OTV.

Furthermore, the optical SF was calculated using Eq. (1)

$$Stopping\ Factor = 10\log_{10}\left(\frac{|E_{Rev}|^2}{|E_{For}|^2}\right) \quad (1)$$

where $|E_{Rev}|^2$ and $|E_{For}|^2$ are the electric field intensities detected at the output port for the reverse- and forward-direction transmissions, respectively. Note that for the forward-direction transmission, the right-hand side is the output port, while for the reverse-direction transmission, the left-hand side is the output port. Here we suppose the intensities of the input EM for both forward- and reverse-direction transmissions are the same. Moreover, the phase of the input EM wave for the forward and backwards incidence cases must be the same.

It is evident from Fig. 3(b) that the maximum SF can be obtained for the linear waveguide with a length of $3a$. Using this obtained optimum length of the linear waveguide connecting both the optical rings effectively increases the SF and the corresponding z-component electric field profile, as shown in Figs. 5(a & b). It is worth noting that the input port is set 20 V/m in E_z for both the forward and reverse configurations operating at 5.279 GHz, where the SF was 47.249dB, which is relatively high compared to the linear waveguide as shown in Fig. 5(c), and most of the conventional PhC and other optical isolators as shown in Table 1. It is essential to note that the positive value for the SF is not typical in conventional FTV. In contrast, in the case of OTV, it is evident from Fig. 5(c) that some resonance peaks show positive and some show negative values for the SF. This effect is solely due to the interference of the EM waves.

To further evaluate the OTV performance at non-resonant frequencies, and to clarify that the reverse excitation strength is not inherently different (a misconception that may arise when observing at resonance frequencies), we focus on the regime where the SF approaches zero, indicating reciprocal behavior. As shown in Fig. 5(c), the SF remains nearly zero in the range 5.40–5.47 GHz. For illustration, 5.438 GHz is selected, and the corresponding electric field maps in Fig. 6 clearly confirm reciprocal behavior under a 20 V/m input for both forward and reverse excitations.

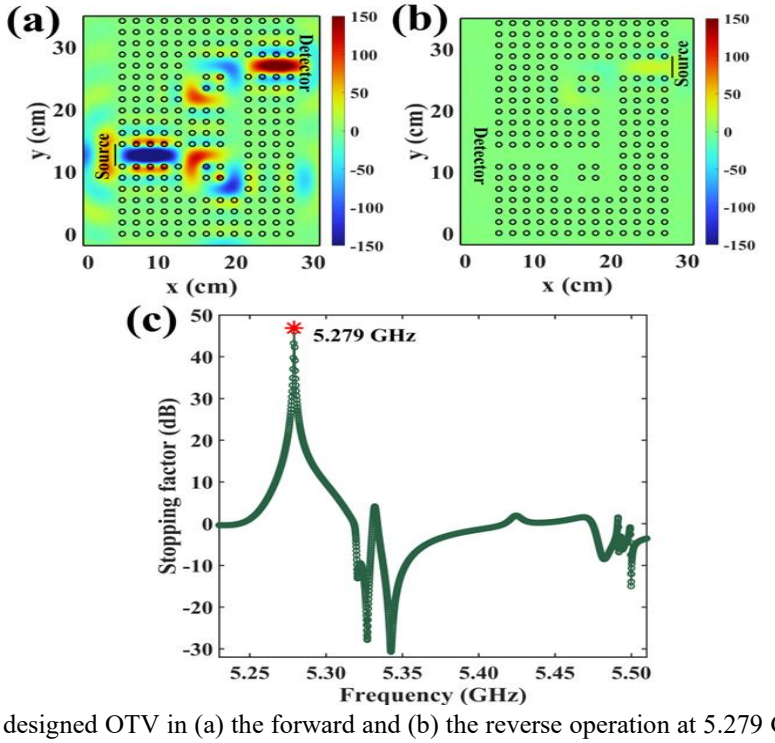

Fig. 5: Ez distribution of the designed OTV in (a) the forward and (b) the reverse operation at 5.279 GHz. (c) Illustration of the SF of the designed OTV.

Table 1: Comparison of the various optical isolators with the proposed unidirectional OTV.

Platform /Material used	Stopping factor (dB)	Applied Magnetic/ Electric Bias	Ref
Silicon	10	No	[42]
Bismuth iron garnet PhC	25	No	[43]
Lithium niobate	25	Electric bias	[44]
Yttrium iron garnet PhC	29	Magnetic bias	[45]
Silicon nitride PhC	28	Magnetic bias	[46]
Silicon nitride platform	32	Magnetic bias	[47]
Silicon	32	Electrical bias	[48]
Silicon	24.5	No	[49]
Alumina PhC	47.2	No	This work

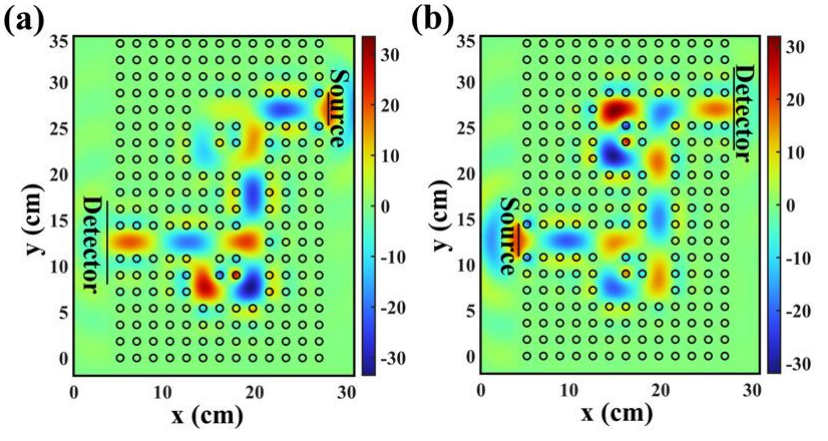

Fig. 6: Distribution of the designed OTV in (a) the forward and (b) the reverse operation at 5.438 GHz.

It is worth noting that the OTV structure shown in Figs. 3 & 5 have asymmetry in the horizontal direction: the left-hand-side port waveguide is between the two cavities, while the right-hand-side waveguide is on top of the two cavities. Such an arrangement is beneficial for coupling waves from the left-side source to the upper and lower cavities. At the same time, it is unfavorable for coupling waves from the right-side source to the lower cavity, as the lower cavity is farther from the right-side source. This contributes to the asymmetrical transmission of photons in the OTV. Furthermore, the left-side waveguide length is 4a, while the right-side waveguide length is 3a. As a result, the left source can couple into the left waveguide in forward transmission more efficiently than the proper source coupling to the right waveguide in reverse transmission. The reason is that the right waveguide of length 3a is equivalent to a transmission line of length 3λ/4, whose equivalent impedance is the impedance Z_w of the waveguide, which doesn't match with the impedance of free space, and thus the coupling of the right-side source to the waveguide is weak, while the left waveguide of 4a is equivalent to a transmission line of length λ=4a, with the load impedance and input impedance being the same as the free-space impedance Z_0, leading to an approximately perfect match between the left open space and the left-side waveguide and thus strong coupling of the left-side source into the left waveguide. Therefore, the proposed structure can work as a unidirectional transmission OTV properly. This impedance matching theory can also explain the existence of negative SF at some frequencies, which corresponds to strong coupling of the right-side source into the OTV and weak coupling of the left-side source into the OTV.

From another perspective, the observed difference in coupling efficiency between the left source and the left waveguide in forward transmission originates from the broken spatial inversion symmetry of the OTV. Through careful design of the OTV, a geometrically asymmetric potential landscape is created, which modifies the overlap integral between the source field and the eigenmodes of the line-defect channel in a direction-dependent manner.

In the case of forward excitation, the left source couples more efficiently into the left waveguide because the local field distribution of the defect mode is well aligned with both the phase and polarization of the source field. The spatial mode profile of the defect supports constructive interference in this direction, thereby maximizing the overlap and enhancing the coupling efficiency. Conversely, under backward excitation,

the phase relation between the source field and the defect mode gives rise to destructive interference, which strongly suppresses the coupling efficiency. This mechanism is further corroborated by the apparent time-reversal symmetry breaking induced by spatial inversion symmetry breaking, as shown in Fig. S1, as detailed in *Supporting Information file*.

From a further point of view, it is well-suited to compare the OTV with the transformational optical (TO) system,[50] which is engineered by continuously varying the spatial dielectric profile. This gradient effective relative permittivity of the TO medium plays a crucial role in wave propagation. When the impedance of the wave and the TO system's boundary match, the wave is allowed to pass smoothly through the medium without reflection. Conversely, an impedance mismatch forbids wave transmission in the opposite direction.

Similarly, the OTV can be interpreted as an effective TO medium. For forward incidence, the structure configuration of the PhC provides an effective impedance profile that is well-suited for the incoming wave to transmit. On the other hand, for the reverse incidence, the effective impedance of the system becomes mismatched, thereby restricting its propagation.

All the simulations carried out in this work were done by the Finite-Element-Method (FEM) based COMSOL Multiphysics Full-wave electromagnetic solver using RF Module.[51] The entire computation domain is assigned the scattering boundary condition, also known as low-reflecting boundary conditions, which provides zero reflection of normal-incidence scattered waves or any other normal-incidence wave, assuming the boundary wall is treated as having zero electric field.

2.2 Experimental setup for the designed PhC-based OTV

The experimental demonstration of the designed OTV was carried out using Alumina (99% pure Al_2O_3) rods with a refractive index of $\varepsilon_r = 9.3987 + 0.0462i$ (ε_r for the rod was calculated using the cavity perturbation technique[51] using a vector network analyzer (VNA)). The experimental setup is shown in Fig. 7(a), where the rods with height h = 4 cm were arranged with a periodicity $0.223a$, with the top and bottom of

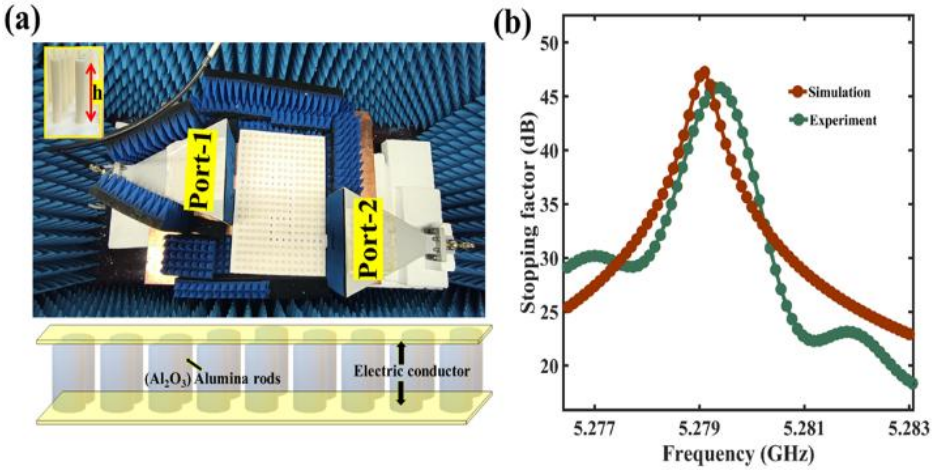

Fig. 7: Experimental setup illustration. (a) Fabricated OTV and (b) the corresponding SF profile.

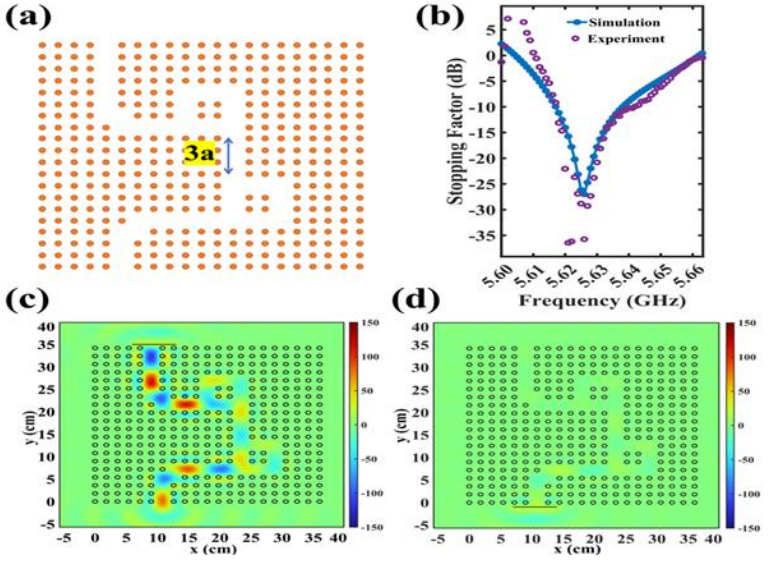

Fig. 8: Additional design. (a) Designed OTV with two circular optical rings. (b) SF for the design shown in 8(a). Electric field z component for (c) forward propagation and (d) reverse blocking.

the PhC array covered by copper sheets to mimic the perfect electric conductor boundary condition and the 2D domain of the simulation. The entire experiment was carried out in an anechoic chamber, which mimics the zero-reflection boundary condition of the simulation. The input EM waves were provided by horn antennas (HD 58HA20). The scattering parameters were measured using a VNA (Agilent E8362B). Fig. 7(b) presents the simulated and experimental SFs, with the structure illustrated in Fig. 3. It is evident from Fig. 7(b) that the experimental data and the simulated data exhibit a near-perfect match.

To further demonstrate the design mechanism and its validity, a different OTV is designed and studied numerically and experimentally, as shown in Fig. 8. It is evident from Fig. 8(b) that the SF of the designed OTV exhibits a sharp resonance, representing its unidirectionality. The mechanism behind the emergence of the unidirectionality is similar to the design shown in Fig. 3. Figs. 8(c & d) illustrates the forward propagation and the reverse blocking of the electric field z component.

3. Results and discussion

3.1 Analogy between EM and hydrodynamics

Using the momentum density carried by the EM fluid, one can derive the fluidic velocity,[52,53] which is indeed analogous to the fluidic velocity in an FTV. A detailed derivation for Eq. (2) is provided in the *Supporting Information file*.

$$\vec{S}_f = \varepsilon\vec{E}\times\vec{B} - \frac{1}{v^2}\left(\frac{1}{2}\varepsilon E^2 + \frac{1}{2\mu}B^2\right)\vec{v} \tag{2}$$

In a "rest-frame" for the EM fluid (i.e. when the net momentum density is zero), $\vec{S}_f = 0$. That is, one requires,

$$\varepsilon\vec{E}\times\vec{B} = \frac{1}{v^2}\left(\frac{1}{2}\varepsilon E^2 + \frac{1}{2\mu}B^2\right)\vec{v} \tag{3}$$

Taking the magnitude of both sides of Eq. (3) and assuming that the fields and $\vec{v}$ lie in the same plane, one finds,

$$\varepsilon\vec{E}\times\vec{B} - \frac{1}{\vec{v}}\left(\frac{1}{2}\varepsilon E^2 + \frac{1}{2\mu}B^2\right) \tag{4}$$

Solving Eq. (4) for $\vec{v}$ gives,

$$\vec{v} = \frac{\left(\frac{1}{2}\varepsilon E^2 + \frac{1}{2\mu}B^2\right)}{\varepsilon\vec{E}\times\vec{B}} \tag{5}$$

This is the velocity of the local EM field (Eq. (5)) of a small EM field element in a small area element; however, to calculate the velocity of EM flow in a waveguide, it can be defined as follows:

$$\vec{s}_1\cdot\vec{v}_{emf} = \frac{\int_S(\vec{v}\cdot\vec{s}_1)\vec{P}\cdot d\vec{s}}{\int_S\vec{P}\cdot d\vec{s}} \tag{6}$$

where, $\vec{v}_{emf}$ is the EM fluid velocity, $\vec{s}_1$ is the unit vector normal to the surface S for integration, and $\vec{P} = \vec{E}\times\vec{B}$.

It is worth noting that the velocity defined by Eq. (6) is actually the photon-flux-weighted average outflowing velocity of the photon stream at the output port surface, measured in the direction normal to the output port surface.

The above (Eq. (6)) emphasizes that the incident EM waves can be well treated as an EM fluid flow through the waveguide. Using (Eq. (6)), the flow velocity of the EM fluid in the structure in Fig. 3(a) is calculated, and the velocity stopping factor (VSF) $20\times\log_{10}\left(v_{reverse}/v_{forward}\right)$ is illustrated in Fig. 9**.** It is evident from Figs. 5 & 9 that the SF calculated using (Eq. (1)) and (Eq. (6)) is well matched, which indicates that the flow of the EM waves inside the designed PhC system works like fluid flow in the conventional TV system.

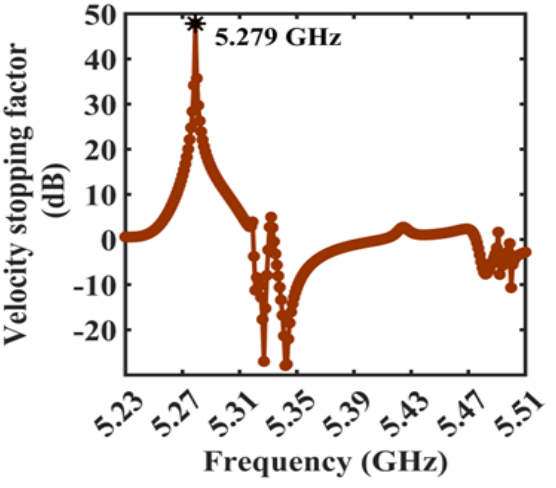

Fig. 9: Illustration of the VSF of the designed OTV.

3.2 Analogue of OTV with fluidic TV

According to quantum theory, an EM wave has wave-particle duality, i.e., it can also be regarded as a stream of photons.

It is pivotal to mention that the fluid flow in an FTV is well explained with the mass conservation equation and the Navier-Stokes equation (Eq. (7 & 8)).

$$\nabla\cdot\vec{u} = 0 \tag{7}$$

$$\frac{\partial\vec{u}}{\partial t} + \vec{u}\cdot\nabla\vec{u} = -\frac{\nabla P}{\rho} + v\nabla^2\vec{u} \tag{8}$$

where, $\vec{u}$,P,ρ and v are the fluid velocity, pressure, density, and kinematic viscosity, respectively.

Whereas Maxwell's wave equation models the flow of EM waves or photon flow.

$$\nabla^2\vec{E} - \frac{\varepsilon\mu}{c^2}\frac{\partial^2\vec{E}}{\partial t^2} = 0 \tag{9}$$

where, ε, μ and c are the relative permittivity, relative permeability, and the speed of light in vacuum.

$$\nabla\cdot\left(\varepsilon\vec{E}\right) = \rho \tag{10}$$

where, ρ is the charge density.

Analogous to fluid flow, the EM wave transport exhibits charge conservation (Eq. (10)). In the classical regime, where the number of photons is very high, a quantum description of photons is not required, as per the correspondence principle. However, for a few photons, treating the EM field as a fluid will not be suitable, and quantum OTV will be an interesting problem to explore further.

The fluid flow in an FTV was characterized by specific parameters, such as the ratio of forward pressure and reverse pressure, which are functions of the fluid velocity $\vec{u}$ as shown in Eq. (8). The flow rate is defined as the volume of fluid that passes through a particular time interval. In the flow modeling, the pressure drops, such as the high pressure drop indicating the forward flow and the low pressure drop denoting the reverse operation, play a crucial role, as the turbulent flow and the laminar flow make a drastic change in the diodicity. Whereas in the OTV, the electric field ($\vec{E}$) (Eq. (9)) plays the role of fluid velocity ($\vec{u}$) (Eq. (8)) in the FTV. The difference between the output and input electric field intensities for the forward and reverse excitations in OTV gives unidirectional transmission property.

4. Conclusion

Combining the wave-particle duality of EM waves in quantum theory, along with the unidirectional transportation property of FTVs, OTVs made of magnet-free linear dielectric were proposed and demonstrated, both numerically and experimentally. The realized OTVs have two optical waveguide ring resonators attached with linear PhC waveguides. In the design, spatial-reversal symmetry is broken, which, for an incident photon stream, is apparently equivalent to time-reversal symmetry breaking, and is responsible for the unidirectional transmission property of the proposed OTVs.

The designed OTV has a maximum SF of 47.249 dB at the frequency regime of 5 – 7 GHz. In the classical regime, the interacting EM waves in sub-wavelength structures can be treated as an EM fluid, allowing us to explain the valve operation with the preexisting mechanism of FTVs. The numerically designed OTV was experimentally demonstrated using Al_2O_3 rods (99% pure) in an air environment. The experiment, as well as the numerical results, yielded a near-perfect match. The OTV demonstrated apparent non-reciprocal transport in a linear photonic-crystal-based passive structure by harnessing interference between coupled resonant modes. The directional response arises purely from structural asymmetry, which breaks spatial inversion symmetry and tailors the interference of multiple scattering pathways. Using only linear, non-magnetic alumina, the device establishes robust one-way light transport that can emerge without invoking magneto-optical bias, nonlinearity, or temporal modulation, highlighting interference engineering as a scalable route to broadband optical diodes within standard photonic platforms.

Unlike the conventional Tesla effect in fluid dynamics, the transmission-stopping direction of EM waves can be different at a different operating frequency with the same OTV structure. This intriguing integration of Tesla's design into the PhC waveguide will gain attention in multi-disciplinary wave-propagation-related domains such as electrodynamics, quantum communication, and acoustics.

Acknowledgments

This research is partially funded by the, National Natural Science Foundation of China (Grant numbers: 61275043, 62205212), Natural Science Foundation of Guangdong Province (Grant number: 2020A1515011154), Natural Science Foundation of Shenzhen City (Grant number: JCYJ20190808151017218), Shenzhen Science and Technology Innovation Commission's Stability Support General Project (Grant number: 20231115111049003), Shenzhen Science and Technology General Program (Grant number: JCYJ20220530114010023), National Key Research and Development Program of China (Grant number: 2023YFF0715303).

Conflict of Interest

There is no conflict of interest.

Supporting Information

Applicable.

CRediT Statement

Zhengbiao Ouyang: Conceptualization. **Zhengbiao Ouyang**, **Asrafali Barkathulla** and **Fahim Khan:** Methodology. **Asrafali Barkathulla**, **Fahim Khan**, **Mi Lin**, **Qiong Wang**, **Keyu Tao** and **Deepika Tyagi:** Data curation. **Zhengbiao Ouyang**, **Yogesh Natesan**, **Asrafali Barkathulla**, **Fahim Khan**, **Mi Lin**, **Qiong Wang** and **Keyu Tao:** Investigation. **Asrafali Barkathulla:** Software. **Zhengbiao Ouyang:** Validation. **Asrafali Barkathulla**, **Zhengbiao Ouyang**, **Yogesh Natesan**, **Fahim Khan** and **Deepika Tyagi:** Visualization. **Zhengbiao Ouyang**, **Suling Shen** and **Qiang Liu:** Funding acquisition. **Zhengbiao Ouyang**, **Suling Shen** and **Qiang Liu:** Project administration. **Zhengbiao Ouyang:** Supervision. **Zhengbiao Ouyang**, **Asrafali Barkathulla**, **Yogesh Natesan** and **Deepika Tyagi:** Writing – Original draft. **Zhengbiao Ouyang**, **Asrafali Barkathulla**, **Yogesh Natesan**, **Suling Shen** and **Qiang Liu:** Writing – Review & editing.

References

[1] P. Walther, K. J. Resch, T. Rudolph, E. Schenck, H. Weinfurter, V. Vedral, M. Aspelmeyer, A. Zeilinger, Experimental one-way quantum computing, *Nature*, 2005, **434**, 169-176, doi: 10.1038/nature03347.

[2] L. Cong, R. Singh, Spatiotemporal dielectric metasurfaces for unidirectional propagation and reconfigurable steering of terahertz beams, *Advanced Materials*, 2020, **32**, 2001418, doi:

10.1002/adma.202001418.
[3] M. A. Ullah, T. Alam, M. S. Alam, S. Kibria, M. T. Islam, A unidirectional 3D antenna for biomedical microwave imaging based detection of abnormality in human body, *Microsystem Technologies*, 2018, **24**, 4991-4996, doi: 10.1007/s00542-018-3919-x.
[4] B. Wu, W. Jiang, J. Jiang, Z. Zhao, Y. Tang, W. Zhou, W. Chen, Wave manipulation in intelligent metamaterials: recent progress and prospects, *Advanced Functional Materials*, 2024, **34**, 2316745, doi: 10.1002/adfm.202316745.
[5] F. D. M. Haldane, S. Raghu, Possible realization of directional optical waveguides in photonic crystals with broken time-reversal symmetry, *Physical Review Letters*, 2008, **100**, 013904, doi: 10.1103/physrevlett.100.013904.
[6] A. Figotin, I. Vitebskiy, Electromagnetic unidirectionality in magnetic photonic crystals, *Physical Review B*, 2003, **67**, 165210, doi: 10.1103/physrevb.67.165210.
[7] Z. Wang, Y. Chong, J. Joannopoulos, M. Soljačić, Physics and applications of one-way magneto-optical photonic crystals, *Conference on Lasers and Electro-Optics*, San Jose, California, USA, 2010, doi: 10.1364/qels.2010.qfh1.
[8] J.-X. Fu, R.-J. Liu, Z.-Y. Li, Robust one-way modes in gyromagnetic photonic crystal waveguides with different interfaces, *Applied Physics Letters*, 2010, **97**, 041112, doi: 10.1063/1.3470873.
[9] A. E. Turner, R. L. Gunshor, S. Datta, New class of materials for optical isolators, *Applied Optics*, 1983, **22**, 3152, doi: 10.1364/ao.22.003152.
[10] F. Auracher, H. H. Witte, A new design for an integrated optical isolator, *Optics Communications*, 1975, **13**, 435-438, doi: 10.1016/0030-4018(75)90140-6.
[11] M. Wang, R.-Y. Zhang, L. Zhang, D. Wang, Q. Guo, Z.-Q. Zhang, C. T. Chan, Topological one-way large-area waveguide states in magnetic photonic crystals, *Physical Review Letters*, 2021, **126**, 067401, doi: 10.1103/physrevlett.126.067401.
[12] H. P. Dizaj, R. Aalipour, S. R. Entezar, Nonreciprocal propagation of optical pulses in a one-dimensional photonic crystal with two Weyl semimetal-based defects, *Journal of Magnetism and Magnetic Materials*, 2024, **589**, 171504, doi: 10.1016/j.jmmm.2023.171504.
[13] S. F. Mingaleev, Y. S. Kivshar, Nonlinear transmission and light localization in photonic-crystal waveguides, *Journal of the Optical Society of America B*, 2002, **19**, 2241, doi: 10.1364/josab.19.002241.
[14] M. SoljaČiĆ, J. D. Joannopoulos, Enhancement of nonlinear effects using photonic crystals, *Nature Materials*, 2004, **3**, 211-219, doi: 10.1038/nmat1097.
[15] C. Caloz, A. Alù, S. Tretyakov, D. Sounas, K. Achouri, Z.-L. Deck-Léger, Electromagnetic nonreciprocity, *Physical Review Applied*, 2018, **10**, 047001, doi: 10.1103/physrevapplied.10.047001.
[16] D. Jalas, A. Petrov, M. Eich, W. Freude, S. Fan, Z. Yu, R. Baets, M. Popović, A. Melloni, J. D. Joannopoulos, M. Vanwolleghem, C. R. Doerr, H. Renner, What is: and what is not: an optical isolator, *Nature Photonics*, 2013, **7**, 579-582, doi: 10.1038/nphoton.2013.185.
[17] L. Feng, M. Ayache, J. Huang, Y.-L. Xu, M.-H. Lu, Y.-F. Chen, Y. Fainman, A. Scherer, Response to comment on nonreciprocal light propagation in a silicon photonic circuit, *Science*, 2012, **335**, 38, doi: 10.1126/science.1213954.
[18] L. Feng, M. Ayache, J. Huang, Y.-L. Xu, M.-H. Lu, Y.-F. Chen, Y. Fainman, A. Scherer, Nonreciprocal light propagation in a silicon photonic circuit, *Science*, 2011, **333**, 729-733, doi: 10.1126/science.1206038.
[19] S. Fan, R. Baets, A. Petrov, Z. Yu, J. D. Joannopoulos, W. Freude, A. Melloni, M. Popović, M. Vanwolleghem, D. Jalas, M. Eich, M. Krause, H. Renner, E. Brinkmeyer, C. R. Doerr, Comment on nonreciprocal light propagation in a silicon photonic circuit, *Science*, 2012, **335**, 38, doi: 10.1126/science.1216682.
[20] E. Bor, M. Turduev, U. G. Yasa, H. Kurt, K. Staliunas, Asymmetric light transmission effect based on an evolutionary optimized semi-Dirac cone dispersion photonic structure, *Physical Review B*, 2018, **98**, 245112, doi: 10.1103/physrevb.98.245112.
[21] C. Wang, X.-L. Zhong, Z.-Y. Li, Linear and passive silicon optical isolator, *Scientific Reports*, 2012, **2**, 674, doi: 10.1038/srep00674.
[22] H. Fei, Q. Zhang, M. Wu, H. Lin, X. Liu, Y. Yang, M. Zhang, R. Guo, X. Han, Asymmetric transmission of light waves in a photonic crystal waveguide heterostructure with complete bandgaps, *Applied Optics*, 2020, **59**, 4416-4421.
[23] Nikola Tesla, Nikola Tesla – Valvular Conduit (Patent), Unites States Patent Office, 1920, 01–16.
[24] W. Li, S. Yang, Y. Chen, C. Li, Z. Wang, Tesla valves and capillary structures-activated thermal regulator, *Nature Communications*, 2023, **14**, 3996, doi: 10.1038/s41467-023-39289-5.
[25] X. Yang, F. Song, Y. Wu, J. Zhou, Z. Yang, Y. Kou, Experimental study on tesla valve and bypass manifold to suppress feedback of rotating detonation engine fuel by kerosene, *Acta Astronautica*, 2023, **211**, 755-763, doi: 10.1016/j.actaastro.2023.07.018.
[26] Q. M. Nguyen, J. Abouezzi, L. Ristroph, Early turbulence and pulsatile flows enhance diodicity of Tesla's macrofluidic valve, *Nature Communications*, 2021, **12**, 2884, doi: 10.1038/s41467-021-23009-y.
[27] D. Stith, The tesla valve–A fluidic diode, *The Physics Teacher*, 2019, **57**, 201, doi: 10.1119/1.5092491.
[28] H. Wang, X. Chen, Optimization of micromixer based on an improved Tesla valve-typed structure, *Journal of the Brazilian Society of Mechanical Sciences and Engineering*, 2022, **44**, 143, doi: 10.1007/s40430-022-03454-6.
[29] M. Xiong, J. Yang, X. Ding, H. Li, H. Zhang, Topology optimization design of micromixer based on principle of Tesla valve: an experimental and numerical study, *Chemical Engineering and Processing - Process Intensification*, 2023, **193**, 109560, doi: 10.1016/j.cep.2023.109560.
[30] F. Gong, X. Yang, X. Zhang, Z. Mao, W. Gao, C. Wang, The study of Tesla valve flow field on the net power of proton

exchange membrane fuel cell, *Applied Energy*, 2023, **329**, 120276, doi: 10.1016/j.apenergy.2022.120276.
[31] S. Wang, J. Hu, H. You, D. Li, Z. Yu, N. Gan, Tesla valve-assisted biosensor for dual-mode and dual-target simultaneous determination of foodborne pathogens based on phage/DNAzyme co-modified zeolitic imidazolate framework-encoded probes, *Analytica Chimica Acta*, 2023, **1275**, 341591, doi: 10.1016/j.aca.2023.341591.
[32] Y. Fan, Z. Wang, X. Xiong, J. Zhu, Q. Gao, H. Wang, H. Wu, Novel concept design of low energy hybrid battery thermal management system using PCM and multistage Tesla valve liquid cooling, *Applied Thermal Engineering*, 2023, **220**, 119680, doi: 10.1016/j.applthermaleng.2022.119680.
[33] S. M. Thompson, T. Jamal, B. J. Paudel, D. K. Walters, Transitional and Turbulent Flow Modeling in a Tesla Valve, *Proceedings of the ASME 2013 International Mechanical Engineering Congress and Exposition. Volume 7B: Fluids Engineering Systems and Technologies*, San Diego, California, USA, November 15–21, 2013, V07BT08A027, doi: 10.1115/IMECE2013-65526.
[34] C. Peng, J. Xu, J. Kumar, H. Almujibah, H. Elhosiny Ali, T. Alkhalifah, S. Alkhalaf, F. Alturise, R. Ghandour, Improving efficiency and optimizing heat transfer in a novel tesla valve through multi-layer perceptron models, *Case Studies in Thermal Engineering*, 2023, **49**, 103391, doi: 10.1016/j.csite.2023.103391.
[35] T. Purdum, 100-Year-Old Tesla Valve Is Cool But Not Well Suited For Industry, Chemical Processing Newsletters, 2021. https://www.chemicalprocessing.com/home/blog/11294002/100-year-old-tesla-valve-is-cool-but-not-well-suited-for-industry.
[36] R. D. Blandford, K. S. Thorne, Modern classical physics, Princeton, *Physics & Astronomy*, Princeton university press, 2018, 671-993, ISBN - 0691159025.
[37] I. Bialynicki-Birula, Photon as a quantum particle, *Acta Physica Polonica B*, 2006, **37**(3), 935–946. https://www.actaphys.uj.edu.pl/R/37/3/935.
[38] L. Wang, L. Lang, W. Ren, Z. Yang, T. Gao, Z. Zhao, M. Kallel, Y. Liu, Electrically insulating composite films with excellent electromagnetic interference shielding performance enabled by multilayer structure, *Engineered Science*, 2025, **37**, 1477, doi: 10.30919/es1477.
[39] L. Lang, W. Ren, J. Men, X. Mao, Z. Yang, S. Zhang, L. Wang, Advances in electromagnetic interference shielding materials with low reflection *Engineered Science*, 2025, **36**, 1640, doi: 10.30919/es1640.
[40] S. Johnson, J. Joannopoulos, Block-iterative frequency-domain methods for Maxwells equations in a planewave basis, *Optics Express*, 2001, **8**, 173, doi: 10.1364/oe.8.000173.
[41] G. Steven, J. D. J. Johnson, Photonic Crystals, *The Road from Theory to Practice*, Springer, New York, 2001, XI-145, ISBN-978-0-7923-7609-5.
[42] K. Goswami, H. Mondal, M. Sen, A. Sharma, Design and analysis of all-optical isolator based on linear photonic crystal, *Brazilian Journal of Physics*, 2022, **52**, 78, doi: 10.1007/s13538-022-01086-8.
[43] K. Fang, Z. Yu, V. Liu, S. Fan, Ultracompact nonreciprocal optical isolator based on guided resonance in a magneto-optical photonic crystal slab, *Optics Letters*, 2011, **36**, 4254-4256.
[44] D. B. Sohn, O. E. Örsel, G. Bahl, Electrically driven optical isolation through phonon-mediated photonic Autler–Townes splitting, *Nature Photonics*, 2021, **15**, 822-827, doi: 10.1038/s41566-021-00884-x.
[45] W. Wang, S. Li, Z. Zhang, Y. Tsuji, Study on Mach-Zehnder optical isolator based on magneto-optic photonic crystal fiber, *Optics Express*, 2025, **33**, 22836, doi: 10.1364/oe.562025.
[46] W. Yan, Z. Wei, Y. Yang, D. Wu, Z. Zhang, X. Song, J. Qin, L. Bi, Ultra-broadband magneto-optical isolators and circulators on a silicon nitride photonics platform, *Optica*, 2024, **11**, 376, doi: 10.1364/optica.506366.
[47] W. Yan, Y. Yang, S. Liu, Y. Zhang, S. Xia, T. Kang, W. Yang, J. Qin, L. Deng, L. Bi, Waveguide-integrated high-performance magneto-optical isolators and circulators on silicon nitride platforms, *Optica*, 2020, **7**, 1555, doi: 10.1364/optica.408458.
[48] D. Huang, P. Pintus, C. Zhang, Y. Shoji, T. Mizumoto, J. E. Bowers, Electrically driven and thermally tunable integrated optical isolators for silicon photonics, *IEEE Journal of Selected Topics in Quantum Electronics*, 2016, **22**, 4403408, doi: 10.1109/JSTQE.2016.2588778.
[49] H. Cheng, Y. Zhou, F. Ruesink, M. Pavlovich, S. Gertler, A. L. Starbuck, A. J. Leenheer, A. T. Pomerene, D. C. Trotter, C. Dallo, M. Boady, K. M. Musick, M. Gehl, A. Kodigala, M. Eichenfield, A. L. Lentine, N. T. Otterstrom, P. T. Rakich, A terahertz-bandwidth non-magnetic isolator, *Nature Photonics*, 2025, **19**, 533-539, doi: 10.1038/s41566-025-01663-8.
[50] B. Asrafali, S. Madhavamoorthi, F. Khan, Z. Ouyang, N. Yogesh, Fabry-Perot modes of the transformation optics (TO)-based cavity and cascaded TO cavities for directional electromagnetic power coupling applications, *Optik*, 2024, **299**, 171601, doi: 10.1016/j.ijleo.2023.171601.
[51] A. Kumar, G. Singh, Measurement of dielectric constant and loss factor of the dielectric material at microwave frequencies, *Progress in Electromagnetics Research*, 2007, **69**, 47-54, doi: 10.2528/pier06111204.
[52] A. I. Arbab, The analogy between electromagnetism and hydrodynamics, *Physics Essays*, 2011, **24**, 254-259, doi: 10.4006/1.3570825.
[53] A. I. Arbab, Is the electromagnetic field in a medium a fluid or a wave, *Optik*, 2017, **130**, 154-161, doi: 10.1016/j.ijleo.2016.10.130.